Femtosecond Optical Vortices in Air

Antoine Vinçotte and Luc Bergé

Département de Physique Théorique et Appliquée, CEA/DAM Ile de France, B.P. 12, 91680 Bruyères-le-Châtel, France

(Received 20 June 2005; published 31 October 2005)

We examine the robustness of ultrashort optical vortices propagating freely in the atmosphere. We first approximate the stability regions of femtosecond spinning pulses as a function of their topological charge. Next, we numerically demonstrate that atmospheric optical vortices are capable of conveying high power levels in air over hundreds of meters before they break up into filaments.

DOI: 10.1103/PhysRevLett.95.193901 PACS numbers: 42.65.Tg, 42.68.Ay, 52.38.Hb

For a decade, the long-range propagation of femtosecond (fs) laser pulses through air [1] has raised increasing interest because of promising applications in lightning discharge control and atmospheric remote sensing [2]. In the self-channeling process, an ultrashort pulse with peak power $P_{\rm in}$, above the self-focusing threshold $P_{\rm cr}$, self-contracts by Kerr effect until its intensity reaches the ionization threshold above which an electron plasma is generated by photo-ionization of air molecules. Plasma tightly defocuses the pulse and the dynamic balance between Kerr focusing and plasma defocusing produces narrow filaments, having $\sim$150 μm diameter and $\sim$1 mJ energy. As isolated entity, a single filament only covers a few meters of propagation in air [3]. In contrast, due to their mutual interaction and energy exchanges, multiple filaments emerging inside powerful (TW) focal spots can maintain the beam envelope localized upon large distances, through the persistence of filamentary clusters initiated by the input beam defects [4].

Because multifilamentation alters the beam homogeneity, several techniques have recently been proposed to organize the fluence patterns, such as introducing astigmatism, amplitude masks, periodic meshes, or even microlenses set along the optical path [5]. Such techniques allowed to control beam configurations engaging low powers in air ($\leq 20P_{\rm cr}$) up to 10 m propagation scales. They, however, do not guarantee to efficiently tame broad pulses decaying into hundreds of filaments at TW power levels and km distances [4,6]. For further developments in atmospheric optics, alternatives for preserving the beam shape over 100 m and beyond are thus welcome.

This alternative may be supplied by optical vortices. Since the pioneering works by Kruglov *et al.* [7], optical vortices have been known as special waveforms exhibiting a dark hole at center and a phase with an integer number of windings, m, called the topological charge of the vortex. They have a doughnut shape distribution and a spiral dislocation of their wave front. From the experimental point of view, vortices are currently generated by use of appropriate phase masks and holographic techniques [8]. Although subject to the azimuthal modulational instability (AMI), they constitute robust structures, which can decay into light cells after covering many diffraction lengths. One reason for their remarkable stability is that spinning beams provide strong attractors of soliton type. As a result, in a medium supporting a cubic-quintic nonlinearity with mixed signs, singly charged ($m = 1$) vortices are linearly stable and may never break up, provided that their associated soliton frequency is high enough [9] (see also Ref. [10] for a review). For the purpose of fs pulses in air, a first investigation [11] discarding time dependencies proposed to use $m = 1$ vortices, in regimes for which plasma saturation competes with the Kerr response of air. Such configurations, nonetheless, rapidly degenerate into filaments. Apart from this preliminary work, the dynamics of pulsed vortex beams self-channeling in the atmosphere has been unexplored so far.

Here, we display evidence of the exceptional robustness of ultrashort optical vortices in air upon propagation ranges *preceding the ionization stage*. We first elaborate on a variational perturbation method approximating the AMI growth rates for cw beams in both saturated and nonsaturated focusing Kerr media. Next, we perform $(2 + 1)$-dimensional simulations validating the previous theory. Finally, direct $(3 + 1)$-dimensional simulations highlight the existence and stability of time-dependent femtosecond optical vortices in air: These objects are capable of conveying high powers quantified by the charge number m, without altering their radial distribution up to hundreds of meters along the propagation axis.

We consider the standard propagation equations [4] governing the electric field envelope $\mathcal{E}(x, y, z, t)$ of fs laser pulses in air and the free electron density $\rho(x, y, z, t)$:

$$\frac{\partial \mathcal{E}}{\partial z} = \frac{i}{2k_0}\nabla_\perp^2 \mathcal{E} + ik_0(n_2\mathcal{R}(t) - n_4|\mathcal{E}|^4)\mathcal{E} - i\frac{k''}{2}\frac{\partial^2}{\partial t^2}\mathcal{E} - \left(\frac{ik_0}{2\rho_c} + \frac{\sigma}{2}\right)\rho\mathcal{E} - \frac{\beta^{(K)}}{2}|\mathcal{E}|^{2K-2}\mathcal{E}, \quad (1)$$

$$\mathcal{R}(t) = \frac{1}{2}\left(|\mathcal{E}|^2 + \tau_K^{-1}\int_{-\infty}^{t} e^{-(t-t')/\tau_K}|\mathcal{E}(t')|^2 dt'\right), \quad (2)$$

$$\frac{\partial \rho}{\partial t} = \sigma_K \rho_{\rm nt}|\mathcal{E}|^{2K} + (\sigma/U_i)\rho|\mathcal{E}|^2. \quad (3)$$

Light pulses are characterized by a beam waist w_0, half-width duration t_p, and central wave number $k_0 = 2\pi/\lambda_0 = \omega_0/c$ at the laser wavelength $\lambda_0 = 800$ nm. In Eq. (1), $\nabla_\perp^2 \equiv \partial_x^2 + \partial_y^2$ and the Kerr response of air $n_2\mathcal{R}(t)$ involves a delayed (Raman) contribution where $n_2 = 4 \times 10^{-19}$ cm^2/W ($P_{\rm cr} \simeq 2.5$ GW) and $\tau_K = 70$ fs. Justified by recent studies [12], a quintic saturation with weak coefficient $n_4 = 2.5 \times 10^{-33}$ cm^4/W^2 has been introduced, which does not prevent plasma generation. Related to the ionization process, $\rho_c \simeq 1.8 \times 10^{21}$ cm^{-3} is the critical plasma density. Plasma defocusing is essentially driven by multiphoton ionization (MPI) of dioxygen molecules with gap potential $U_i = 12.1$ eV and neutral density $\rho_{\rm nt} = 5.4 \times 10^{18}$ cm^{-3}. It involves the MPI rate $\sigma_K = 2.9 \times 10^{-99}$ s^{-1} cm^{2K}/W^K and number of photons $K = 8$, and induces multiphoton absorption (MPA) with coefficient $\beta^{(K)} \simeq 3.1 \times 10^{-98}$ cm^{2K-3}/W^{K-1}. Eqs. (1) and (3) also include avalanche ionization ($\sigma = 5.4 \times 10^{-20}$ cm^{-2}) and group-velocity dispersion (GVD) with $k'' = 0.2$ fs^2/cm.

Stable spinning solitons are already known to exist in (3 + 1)-dimensional geometry, whenever GVD is anomalous ($k'' < 0$) and nonlinearities are noninertial [13]. In that case, stationary vortices exhibit a torus shape in the (x, y, t) space. The purpose is different here, since GVD is normal ($k'' > 0$), which counteracts the formation of localized stationary ground states. To overcome this limitation, we shall henceforth consider an input pulse with large enough duration, $t_p = 250$ fs, in order to reject the dispersion length $\sim t_p^2/k''$ to kilometer distances. With large t_p, the temporal pulse profile may not undergo a significant broadening, which could decrease the vortex power early and provoke a premature beam spreading. This condition justifies the omission of space-time focusing and self-steepening in Eqs. (1)–(3), since $\omega_0 t_p \gg 1$.

Before proceeding with (3 + 1)-dimensional numerical simulations, we first study vortex dynamics in the framework of a reduced (2 + 1)-dimensional model, successfully used in Ref. [6] to describe the multifilamentation of broad, TW beams for weak avalanche ionization, $\sigma \to 0$. Using the ansatz $\mathcal{E}(x, y, z, t) = \psi(x, y, z) \times e^{-[t-t_c(z)]^2/T^2}$ where $T \simeq t_p/10$ in plasma regime, we average in time Eqs. (1)–(3) following the procedure of Ref. [6] and get rid of the GVD term by a trivial phase shift. This method amounts to freezing the pulse in time, which provides a cw version of the original model equations. The spatial envelope ψ is then described in dimensionless form by the extended nonlinear Schrödinger (NLS) equation

$$i\partial_z\psi + \nabla_\perp^2\psi + f(|\psi|^2)\psi + i\nu|\psi|^{2K-2}\psi = 0, \qquad (4)$$

$$f(|\psi|^2) = \alpha|\psi|^2 - \epsilon|\psi|^4 - \gamma|\psi|^{2K}, \qquad (5)$$

by means of the substitutions $z \to 4z_0 z$, $t \to tt_p$, $(x, y) \to (x, y)w_0$, $\psi \to \sqrt{P_{\rm cr}/4\pi w_0^2}\psi$, and $\rho \to (\rho_c/2z_0k_0)\rho$, where $z_0 = \pi w_0^2/\lambda_0$ denotes the Rayleigh length for Gaussian beams. Here, only α and γ vary with t_p. For the duration $t_p = 250$ fs, the coefficients of Eq. (4) take the values $\alpha = 0.446$, $\epsilon = 7.3 \times 10^{-7}$[cm^2]$/w_0^2$, $\gamma = 8.4 \times 10^{-40}$[cm$^{2(K-1)}$]$/w_0^{2(K-1)}$, and $\nu = 1.2 \times 10^{-35}$[cm$^{2(K-2)}$]$/w_0^{2(K-2)}$ with w_0 expressed in cm.

From Eqs. (4) and (5), we develop a perturbative analysis for vortex rings subject to AMI in the limit of weak MPA, $\nu \to 0$ [4]. On the one hand, as the beam is expected to quickly converge towards an exact vortex profile, spinning modes are approximated by means of trial functions in the form $\psi_m = A_m r^{|m|}\exp(-r^2/(2a_m^2) + im\theta + i\lambda z)$, where $r = \sqrt{x^2 + y^2}$, θ is the azimuthal angle and λ the vortex soliton parameter. The normalized amplitude A_m and waist a_m are determined by solving the variational problem $\delta(H_m + \lambda P_m) = 0$, where $P_m = 2\pi\int_0^{+\infty}|\psi_m|^2 rdr$ and $H_m = 2\pi\int_0^{+\infty}\{|\partial_r\psi_m|^2 + m^2|\psi_m|^2/r^2 - \int_0^{|\psi_m|^2} f(u)du\}rdr$ are the power and Hamiltonian of the vortex, respectively. For the cubic-quintic NLS equation ($\gamma = 0$), solving for A_m and a_m provides relatively good approximations of the genuine vortex modes [7,9]. On the other hand, we extend the perturbative procedure of Ref. [14] to ring-shaped solutions carrying a nonzero charge m: We consider perturbations acting along a ring of mean radius $\bar{r}_m = [\int r^2|\psi_m|^2 d\vec{r}/P_m]^{1/2}$. Assuming constant intensity and spatial uniformity for this ring, we rewrite the diffraction operator as $\nabla_\perp^2 = \partial_s^2$ with $s = \bar{r}_m\theta$ and search for the growth rate, $\mathrm{Im}(\mu)$, of azimuthal perturbations entering the solution $\psi = (\psi_0 + \delta\psi_1 e^{i\mu z + iM\theta} + \delta\psi_2^* e^{-i\mu^* z - iM\theta}) \times e^{i\lambda z + im\theta}$. Elementary algebra yields

$$\mathrm{Im}(\mu) = \frac{M}{\bar{r}_m}\left[2f'(|\psi_0|^2)|\psi_0|^2 - \frac{M^2}{\bar{r}_m^2}\right]^{1/2}, \qquad (6)$$

where $f'(u) \equiv \partial_u f$ and M denotes the azimuthal index of the perturbation. All required information about the charge m of the input vortex lies in the dependencies of ψ_0, taken as $\psi_0 = \psi_m(r = \bar{r}_m)$. Figure 1(a) illustrates this growth rate as a function of M in the academic case of a cubic-

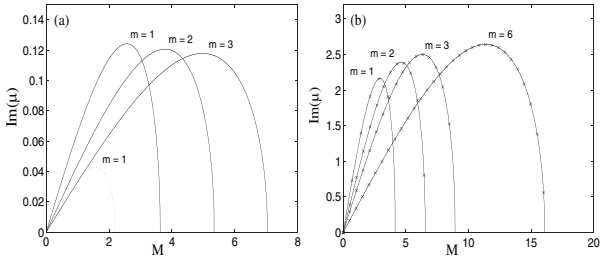

FIG. 1. AMI growth rates of 2D NLS vortices (a) in the cubic-quintic limit $\alpha = \epsilon = 1$ (solid curves: $\lambda = 0.1$; dotted curve: $\lambda = 0.14$ for $m = 1$); (b) in the cubic case $\lambda = 1$ for $\alpha = 0.446$, $\epsilon = 0$. Vortex charges m are indicated next to the curves. In (b), cross symbols mark the points calculated from Eqs. (4) and (5) with $\nu = 0$, $t_p = 250$ fs, and $w_0 = 3$ mm.

quintic nonlinearity $\alpha = \epsilon = 1$ ($\gamma = \nu = 0$). As only integer values of M are physically relevant, we observe that AMI takes place at a maximal azimuthal index $M_{\max} \approx 2|m|$ for the soliton parameter $\lambda = 0.1$. For singly charged vortices, the growth rate significantly diminishes as λ increases. Stability follows [$\mathrm{Im}(\mu) = 0$] as soon as λ exceeds the critical point $\lambda_{\mathrm{cr}} \simeq 0.147$, from which $f'(|\psi_0|^2) < 0$. These preliminary results recover those inferred from numerical shooting techniques [9–11]. The present procedure, of course, suffers some approximation, but it yields—for the first time—a clear dependency of the optimal perturbation index $M_{\max}$ over the vortex charge m. Figure 1(b) supplies similar information for the purely cubic NLS equation, in which $\alpha = 0.446$, $\epsilon = \gamma = 0$, and the soliton parameter λ can be set equal to unity without loss of generality. In this case, the AMI growth rate becomes larger, with maxima attained at $M_{\max} \approx 2|m| + 1$. In the same figure, cross symbols indicate the values of $\mathrm{Im}(\mu)$ computed from the complete function Eq. (5) for the realistic waist $w_0 = 3$ mm and $t_p = 250$ fs. Because these parameters make quintic and MPI saturations very small, Eq. (4) is close to the purely cubic NLS equation, which explains why these data superimpose with the curves of Fig. 1(b).

To check these behaviors, we performed direct numerical integrations of Eqs. (4) and (5) from the pulse parameters corresponding to the cross symbols of Fig. 1(b). The results expressed in physical units are summarized in Fig. 2. For given m, the initial condition was chosen as the above Gaussian ansatz ψ_m perturbed by 10% amplitude random noise. The input beams possess a physical power close to $P_m \simeq 2^{2|m|} P_{\mathrm{cr}} |m|!(|m| + 1)!/[\alpha(2|m|)!]$, a mean radius $\bar{r}_m \simeq (|m| + 1)w_0$, and intensity $A_m^2 = P_m/[\pi w_0^2 |m|!(|m| + 1)^{|m|+1}]$. They rapidly relax onto a vortex ground state, which keeps its shape over long distances (> 200 m). The singly charged vortex with $P_1 \simeq 9P_{\mathrm{cr}}$, attained in Fig. 2(a), propagates over several hundreds of meters, before undergoing 2–3 azimuthal modulations. With $|m| \geq 2$ [Fig. 2(b)], $(2|m| + 1)$ modulations break the vortex ring. The number of modulations issued from AMI is thus in excellent agreement with the predictions of Fig. 1(b). Note that the filamentation stage occurs earlier as the value of m is augmented.

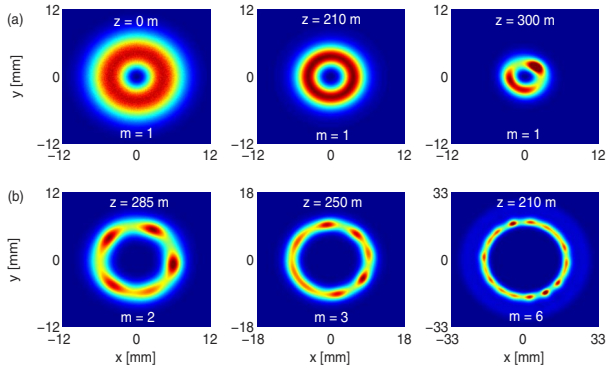

FIG. 2 (color online). Vortex profiles with $w_0 = 3$ mm and $t_p = 250$ fs ($\alpha = 0.446$) computed from Eqs. (4) and (5) for (a) $m = 1$, $P_{\mathrm{in}} = 9P_{\mathrm{cr}}$, (b) $m = 2$, $P_{\mathrm{in}} = 17.9P_{\mathrm{cr}}$; $m = 3$, $P_{\mathrm{in}} = 28.7P_{\mathrm{cr}}$, and $m = 6$, $P_{\mathrm{in}} = 69.6P_{\mathrm{cr}}$. Note the change of scales.

From now on we analyze (3 + 1)-dimensional situations, where the former vortices exhibit a temporal distribution. For further comparison, Fig. 3(a) illustrates the fluence ($\mathcal{F} \equiv \int_{-\infty}^{+\infty} |\mathcal{E}|^2 dt$) of pulses computed numerically from Eqs. (1)–(3) with the super-Gaussian input $\mathcal{E}_0 = A_{\mathrm{in}} e^{-r^3/w_0^3 - t^2/t_p^2}$ perturbed by a 10% random noise and having the averaged power $P_{\mathrm{in}} \simeq 70P_{\mathrm{cr}}$. Such pulses are currently employed in meter-range propagation experiments [1]. Here, they develop a ringlike diffraction pattern which becomes unstable with 7 modulations after 2.5 m of propagation only. Another example in Fig. 3(b) shows the fluence pattern of an optical doughnut with input profile $\mathcal{E}_0 = A_{\mathrm{in}}(r/w_0) e^{-r^2/w_0^2 - t^2/t_p^2 + i\theta}$ and same power $P_{\mathrm{in}} \simeq 70P_{\mathrm{cr}}$, which does not belong to the class of vortex solitons. This beam, although more robust, cannot avoid AMI that induces ~12 modulations focusing into a similar number of filaments over a few meters.

Let us now examine guenuine vortex solitons. To create them, we plug into Eqs. (1) and (3) initial conditions in the form $\mathcal{E}(z = 0) = A_m(r/w_0)^{|m|} \exp[-r^2/(2\bar{r}_m^2) - t^2/t_p^2 + im\theta]$, which we again perturb by a 10% random noise. The amplitude A_m and radius $\bar{r}_m$ are computed from the above variational method. Such beam configurations should thus converge to a radial (2D) vortex profile and are henceforth called *femtosecond optical vortices* (FOVs). Results from numerical simulations are presented in Fig. 4. Whereas singly humped or arbitrary ringlike distributions decay into filaments at moderate distances <10 m [Fig. 3], remarkably, FOVs propagate beyond 100 m, before breaking up into filaments. This property applies to low-power ($P_1 \simeq 9P_{\mathrm{cr}}$), singly charged ($m = 1$) vortices shown in Figs. 4(a) and 4(b), where the first subplot of Fig. 4(b) illustrates the radial shape of the vortex reached from the perturbed input beam. Three modulations affect the vortex. They give rise to three filaments that grow up and produce an electron plasma at $z \simeq 130$ m, when their fluence exceeds ~0.2 J/cm^2. The final filaments rotate and do not fuse, because all of them must preserve the total angular momentum of the incident beam [10]. The same property

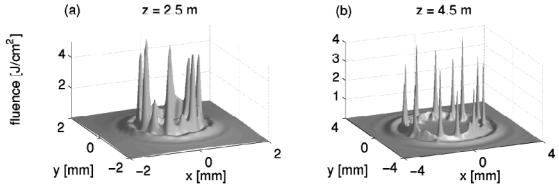

FIG. 3. (3 + 1)-dimensional fluence patterns of beams with $w_0 = 3$ mm and $t_p = 250$ fs having (a) a super-Gaussian shape and (b) an arbitrary ring-shaped profile with $m = 1$.

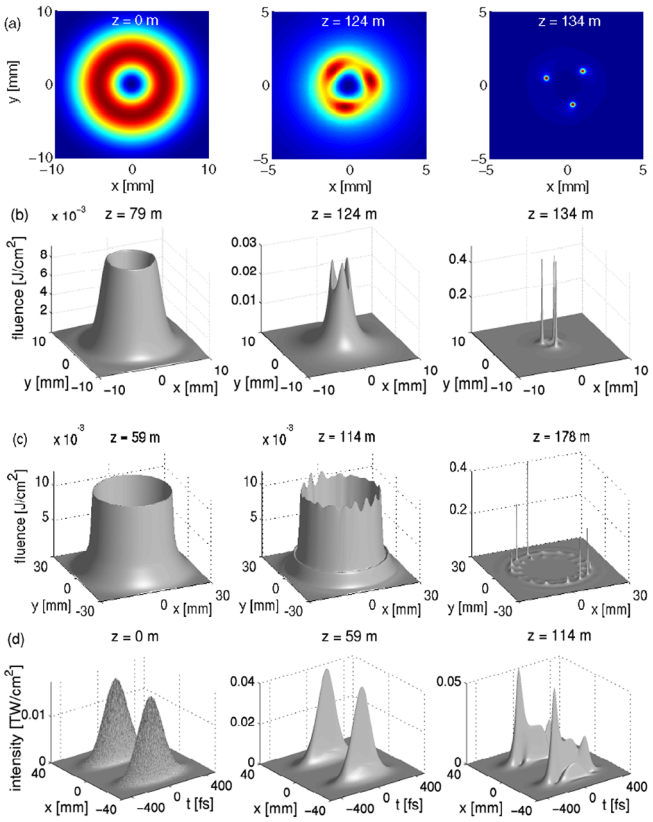

FIG. 4 (color online). Fluences of vortex profiles with 3 mm waist and 250 fs duration computed from Eqs. (1)–(3) for (a), (b) $m = 1$ and $P_1 = 9P_{\mathrm{cr}}$, (c) $m = 6$ and $P_6 = 69.6P_{\mathrm{cr}}$. Row (d) details pulse distortions in the plane $(x, y = 0, t)$ for this latter case. Note the change of scales and propagation distances.

applies to high-power vortices. Figure 4(c) depicts different propagation stages of FOVs with $m = 6$ ($P_6 \simeq 70P_{\mathrm{cr}}$). Again, the input beam attains a vortex state that holds its shape at large distances. Beyond $z = 100$ m, AMI starts and forms about 13 modulations. These amplify about 8 filaments which ionize the medium from $z \geq 175$ m. Compared with Fig. 3, the onset distance of filamentation differs between a simple ring profile and a genuine vortex mode. Two reasons explain this feature: (i) The growth rate $\mathrm{Im}(\mu)$ for the initial profiles used in Fig. 3 is $\sim$24 times higher than that of the vortex mode in Fig. 1(b). (ii) The diffraction length dictating the self-focusing range for the vortex solitons is proportional to $\bar{r}_m^2$, which increases with m. Note that the number of filaments still agrees with the above AMI theory. For vortices with $m = 1$ as well as $m = 6$, differences in the characteristic distances of multifilamentation occur between $(2 + 1)$ [Fig. 2] and $(3 + 1)$ [Fig. 4] dimensional simulations, because the averaged-in-time model [Eq. (4)], limited to one short time slice, overestimates the nonlinear focus at which filaments start to develop. This point, linked to the value of α, was already reported in Ref. [6]. Figure 4(d) details the temporal profile of the pulse along the line $y = 0$. Before the onset distance of AMI ($z = 114$ m), the distribution in time does not significantly evolve, which maintains the vortex shape stable over long distances, as expected.

In conclusion, we have revealed that new types of vortex configurations (FOV) are able to guide ultrashort pulses over considerable distances in the atmosphere, before the filamentation instability takes place. Nowadays, optical vortices can easily be prepared experimentally [8]. Because their power is quantified as a function of the vortex charge, FOVs can be used as powerful tools to transmit specific high energy levels within a robust shape. Their feasibility opens new trends in the techniques of remote filaments induced breakdown spectroscopy [15], which exploits ionizing femtosecond channels to probe aerosols, bioaerosols, as well as solid materials at remote distances. Controlling the onset of filamentation over long ranges is a key issue in this field, which could be achieved by means of optical vortices.

[1] A. Braun *et al.*, Opt. Lett. **20**, 73 (1995); A. Couairon *et al.*, J. Opt. Soc. Am. B **19**, 1117 (2002).
[2] L. Wöste *et al.*, Laser Und Optoelektronik **29**, 51 (1997); J. Kasparian *et al.*, Science **301**, 61 (2003).
[3] F. Courvoisier *et al.*, Appl. Phys. Lett. **83**, 213 (2003); S. Skupin *et al.*, Phys. Rev. Lett. **93**, 023901 (2004).
[4] M. Mlejnek, M. Kolesik, J. V. Moloney, and E. M. Wright, Phys. Rev. Lett. **83**, 2938 (1999); L. Bergé *et al.*, Phys. Rev. Lett. **92**, 225002 (2004).
[5] G. Fibich, S. Eisenmann, B. Ilan, and A. Zigler, Opt. Lett. **29**, 1772 (2004); G. Méchain *et al.*, Phys. Rev. Lett. **93**, 035003 (2004); K. Cook *et al.*, Appl. Phys. Lett. **86**, 021105 (2005); V. P. Kandidov *et al.*, Appl. Phys. B **80**, 267 (2005).
[6] S. Skupin *et al.*, Phys. Rev. E **70**, 046602 (2004).
[7] V. I. Kruglov and R. A. Vlasov, Phys. Lett. A **111**, 401 (1985); V. I. Kruglov, Yu. A. Logvin, and V. M. Volkov, J. Mod. Opt. **39**, 2277 (1992).
[8] N. R. Heckenberg, R. McDuff, C. P. Smith, and A. G. White, Opt. Lett. **17**, 221 (1992); V. Tikhonenko, J. Christou, and B. Luther-Davies, Phys. Rev. Lett. **76**, 2698 (1996); D. V. Petrov *et al.*, Opt. Lett. **23**, 1444 (1998).
[9] M. Quiroga-Texeiro and H. Michinel, J. Opt. Soc. Am. B **14**, 2004 (1997); V. I. Berezhiani, V. Skarka, and N. B. Aleksić, Phys. Rev. E **64**, 057601 (2001); I. Towers *et al.*, Phys. Lett. A **288**, 292 (2001).
[10] A. S. Desyatnikov, Yu. S. Kivshar, and L. Torner, Prog. Opt. **47**, 291 (2005).
[11] V. Skarka, N. B. Aleksić, and V. I. Berezhiani, Phys. Lett. A **319**, 317 (2003).
[12] A. Vinçotte and L. Bergé, Phys. Rev. A **70**, 061802 (2004); L. Bergé *et al.*, Phys. Rev. E **71**, 016602 (2005).
[13] D. Mihalache *et al.*, Phys. Rev. E **61**, 7142 (2000); D. Mihalache *et al.*, Phys. Rev. Lett. **88**, 073902 (2002).
[14] J. M. Soto-Crespo, E. M. Wright, and N. N. Akhmediev, Phys. Rev. A **45**, 3168 (1992).
[15] K. Stelmaszczyk *et al.*, Appl. Phys. Lett. **85**, 3977 (2004).